

**United States
Department of
Agriculture**

**Natural Resources
Conservation
Service**

**11 Campus Boulevard,
Suite 200
Newtown Square, PA 19073**

Subject: SOI – Geophysical Field Assistance

Date: 28 March 2008

To: Dr. Henry Lin
Assistant Professor of Hydropedology/Soil Hydrology
Crop & Soil Sciences Department
415 Agricultural Sciences and Industries Building
Pennsylvania State University
University Park, PA 16802

Edgar White
State Soil Scientist
USDA-NRCS
One Credit Union Place, Suite 340
Harrisburg, PA 17110-2993

Purpose:

Electromagnetic induction (EMI) surveys were completed at the Pennsylvania State University's Klepler Farm (10 March 2008) in Centre County, and within the Shale Hills Catchment (20 and 21 March 24, 2008) in northern Huntingdon County, Pennsylvania. In addition, a small grid was setup within the Shale Hills Catchment to further evaluate the utility of two ground-penetrating radar (GPR) processing and imaging software programs: *GPR-SLICE* and *RADAN*. Training was also provided to Ken Takagi on the operation of an EM38 meter. This meter has been loaned to the Pennsylvania State Hydropedology Team for research within the Shale Hills Catchment.

Activities:

Field activities were completed on 10 (Klepler Farm), and 20 and 21 (Shale Hill Catchment) March 2008.

Participants:

Jim Doolittle, Research Soil Scientist, USDA-NRCS-NSSC, Newtown Square, PA
Henry Lin, Assistant Professor of Hydropedology/Soil Hydrology, Department of Crop & Soil Sciences, PSU, University Park, PA
Ken Takagi, Graduate Student, Department of Crop & Soil Sciences, PSU, University Park, PA
Jun Zhang, PhD Student, Department of Crop & Soil Sciences, PSU, University Park, PA
Quing Zhu, PhD Student, Department of Crop & Soil Sciences, PSU, University Park, PA

Recommendations:

1. An EM38 meter (Serial number: 9728005; AG number 269) has been loaned to Ken Takagi and the Hydropedology Team of the Department of Crop & Soil Sciences, Pennsylvania State University, for the purpose of conducting electromagnetic surveys within the Shale Hills Catchment. Over the next four months, periodic EMI surveys will be conducted over small grid sites located within the catchment. The purpose of these surveys is to refine EMI survey protocol over very resistive soils and to assess the short-range (large scale) spatiotemporal patterns in apparent conductivity (EC_a) and soil water content.
2. The second, bi-monthly EMI survey was completed over selected research fields at Klepler Farm. The purpose of these surveys is to assess broad (small scale) spatiotemporal patterns in EC_a , define hydropedological functional units, and correlate EC_a with soil properties. This survey resulted in a large number of exceptionally low to negative EMI responses with the EM38DD meter operated in the horizontal dipole orientation. While

measurements obtained in the both dipole orientations followed similar trends in magnitudes, they were not as closely associated ($r = 0.51$) as experienced in previous studies. Because of the large number of negative readings in the horizontal dipole orientations, and the reduced collinearity between measurements obtained in the horizontal and vertical dipole orientations, the EM38DD meter has been returned to Geonics Limited for calibration and testing.

3. Results of the reconnaissance EMI survey at the Shale Hills Catchment were disappointing. Unusually poor satellite reception resulted in the loss of many data points. As a consequence, the data population was small and significant portions of the catchment lacked EC_a data. This resulted in more generalized interpolations of data and broader, less intricate spatial EC_a patterns. In addition, because of exceptionally poor satellite reception in the lower portions of the catchment, areas of higher EC_a that normally occurred along the stream channel were not shown on the summary plots. Also, in contrast to the previous three EMI reconnaissance surveys of the catchment, multiple traverses were not conducted across and along swales. These landforms often had areas of higher EC_a . As a consequence of this sampling plan, the swales are indistinguishable on the plot of EC_a data.
4. In order for Jun Zhang to further experiment and access the processing techniques contained in *GPR-SLICE*, a small, detailed grid site was established on the lower portion of a swale located within the Shale Hills Catchment. Two GPR surveys were completed in orthogonal directions across this grid site.
5. A wetting experiment was completed with a 400 MHz antenna in an area of Weikert soils within the Shale Hills Catchment. This brief study is a prelude to more intensive investigations scheduled later this year with PSU's Geophysical Department.

It was my pleasure to participate in these studies and to work with the graduate students at Pennsylvania State University.

With kind regards,

James A. Doolittle
 Research Soil Scientist
 National Soil Survey Center

cc:

- B. Ahrens, Director, National Soil Survey Center, USDA-NRCS, Federal Building, Room 152, 100 Centennial Mall North, Lincoln, NE 68508-3866
- S. Carpenter, MLRA Office Leader, USDA-NRCS, 75 High Street, Room 301, Morgantown, WV 26505
- M. Golden, Director, Soil Survey Division, USDA-NRCS, Room 4250 South Building, 14th & Independence Ave. SW, Washington, DC 20250
- W. Tuttle, Soil Scientist (Geophysical), National Soil Survey Center, USDA-NRCS, P.O. Box 60, 207 West Main Street, Rm. G-08, Federal Building, Wilkesboro, NC 28697
- L. West, National Leader for Soil Survey Investigations, National Soil Survey Center, USDA-NRCS, Federal Building, Room 152, 100 Centennial Mall North, Lincoln, NE 68508-3866

Electromagnetic Induction Surveys:

Materials and Methods:

The EM38 and EM38DD meters, manufactured by Geonics limited (Mississauga, Ontario) were used in the investigations discussed in this report.¹ These meters require only one person to operate. No ground contact is required with either instrument. Both meters have a 1-m intercoil spacing and operate at a frequency of 14,600 Hz. The EM38 meter weighs about 1.4 kg (3.1 lbs). Operating procedures for the EM38 meter are described by Geonics Limited (1998). The EM38DD meter consists of two, coupled EM38 meters. This instrument weighs about 2.8 kg (6.2 lbs). Operating procedures for the EM38DD meter are described by Geonics Limited (2000). When placed on the soil surface, these meters provide theoretical penetration depths of about 0.75 and 1.5 m in the horizontal and vertical dipole orientations, respectively. These meters measure the apparent conductivity (EC_a) of earthen materials, which is expressed in milliSiemens/meter (mS/m).

Within the Shale Hills Catchment, station-to-station and continuous surveys were completed with the lighter-weight EM38 meter. The high-intensity survey at Klepler Farm was completed with an EM38DD meter operated in the continuous mode. To complete the EMI survey at Klepler Farm, the EM38DD was placed in a plastic sled and towed behind an all-terrain vehicle (ATV). An Allegro CX field computer (Juniper Systems, North Logan, UT) was used to record and store both EMI and position data. The coordinates of each EC_a measurement were recorded with a Trimble AgGPS114 L-band DGPS (differential GPS) antenna (Trimble, Sunnyvale, CA).¹ The DAT38W, Trackmaker38DD, and Trackmaker38 software programs developed by Geomar Software Inc. (Mississauga, Ontario) were used to record, store, and process EC_a and GPS data.¹

In order to make temporal comparisons of EC_a measurements, it is recommended that all data be corrected to a standard temperature. Apparent conductivity increases with soil temperature. As the soil temperature rises, the soil water become less viscous and dissolved ions become more mobile. This results in higher EC_a values (McNeill, 1980). As it is impractical to account for variations at each point and at different soil depths, the correction factor is often based on a single measurement made at a depth of 50 cm. At Klepler Farm (10 March), the surface layers were frozen and the soil temperature at a depth of 50 cm was 0.56 °C (33 °F). Temperatures are continuously monitored within the Shale Hill Catchment. At a representative site, for 20 and 21 March, temperatures averaged 3.7 °C (38.7 °F) at a depth of 84 cm. Based on these temperatures, all EC_a data shown in this report have been corrected to a standard temperature of 24° C (75° F) using equation [1] from Handbook 60 (U.S. Salinity Laboratory Staff, 1954):

$$EC_{25}=f_t EC_t \quad [1]$$

where, f_t is a temperature conversion factor.

To help summarize the results of the EMI surveys, SURFER for Windows (version 8.0), developed by Golden Software, Inc. (Golden, CO), was used to construct the simulations shown in this report.² Grids of EC_a data were created using kriging methods with an octant search.

Survey Procedures:

Pedestrian and mobile EMI surveys were completed at Shale Hills Catchment and Klepler Farm, respectively. For most surveys, the EMI meters were operated in the continuous mode with measurements recorded at a 1-sec interval. Meters were orientated with their long axis parallel to the direction of travel. In the Shale Hills Catchment, where possible, the EM38 meter was held about 5 cm (2 inches) above the ground surface. However, steep slopes, tree limbs, and ground cover made walking difficult and caused the meter to vary slightly in height. Where possible, traverses were conducted parallel to the slope contours. Horizon obstructions, satellite shading, and multipath reception reduced the accuracy and reliability of GPS positioning within the Shale Hills Catchment, especially on lower slopes and beneath the evergreen canopy along the lower reach of the stream channel.

Within the Shale Hills Catchment, EC_a measurements were collected at a large number of time-domain reflectometry (TDR) monitoring sites by Ken Takagi. For these measurements, the EM38 meter was operated in the *station-to-station*

¹ Manufacturer's names are provided for specific information; use does not constitute endorsement.

² Manufacturer's names are provided for specific information; use does not constitute endorsement.

mode. At each TDR monitoring site, the meter was placed on the soil surface and two measurements (each orthogonal to the other) were obtained in each dipole orientation (vertical and horizontal).

At Klepler Farm, the EM38DD meter was towed behind an ATV in a plastic sled at speeds of 1 to 3 m/sec. The EMI survey of Klepler Farm was completed by driving the ATV at a uniform pace along crop rows, in a random or back and forth manner.

Results:

1. Klepler Farm:

Table 1 summarizes the results of the EMI survey that was completed on the research fields at Klepler Farm. The relatively low EC_a recorded across these fields reflect the electrically resistive nature of soils and underlying limestone bedrock. For the shallower-sensing (0 to 75 cm) horizontal dipole orientation (HDO), EC_a ranged from about -13 to 510 mS/m. The large range in EC_a values reflects the presence of buried utility lines and artifacts within these fields. In the HDO, EC_a averaged 5.43 mS/m with a standard deviation of 7.98 mS/m. One-half the EC_a measurements recorded in the HDO were between 1.70 and 9.15 mS/m. For the deeper-sensing (0 to 150 cm) vertical dipole orientation (VDO), EC_a ranged from about -96 to 68 mS/m. Once again, the large range in EC_a reflects the presence of buried artifacts. In the VDO, EC_a averaged 11.46 mS/m with a standard deviation of 4.64 mS/m. One-half the EC_a measurements recorded in the VDO were between 8.50 and 14.46 mS/m.

Table 1

Basic EMI Statistics for the EMI surveys conducted at the Klepler Farm Research Site on 16 January and 11 March 2008.

(Other than the number of observations, all values are expressed in mS/m)

	JAN	JAN	MAR	MAR
	HDO	VDO	HDO	VDO
Number	8274	8274	7344	7344
Minimum	8.46	-203.58	-13.18	-96.33
25%-tile	21.58	22.43	1.70	8.50
75%-tile	26.66	27.09	9.15	14.46
Maximum	266.44	105.61	509.67	68.26
Average	24.67	25.41	5.43	11.46
Standard. Deviation	8.45	8.33	7.98	4.64

The range in EC_a was affected by the presence of buried utility lines within the fields. Buried power cables followed the northern field boundary and entered the south-central portion of the study site along a farm road. These utilities produced electromagnetic interference resulting in anomalous EMI responses. In addition, some anomalous EC_a values are attributed to metallic artifacts that were discarded or buried in the field and crossed or closely approached with the meter during the survey.

A large number of negative EC_a measurements were recorded with the EM38DD meter in the HDO. Most of these measurements were located on higher-lying areas where the depth to bedrock was shallow and the earthen materials were exceptionally resistive. For most earthen materials, EC_a is expected to be inherently non-negative. Many have used nonnegativity constraints in modeling and mapping spatial EC_a patterns [either adjusting all numbers or removing negative data points] (Hendrickx et al., 2002). The EM38DD meter was calibrated on a lower-lying slope position, where the soils were deeper and slightly more conductive than on higher-lying areas. Had the meter been calibrated on a ridge top where the depth to bedrock was shallower, the meter could have been forced to show positive numbers, but similar spatial results would have been obtained. The selection of a known “calibration site” within these fields could help to insure consistency among the EMI surveys, which will be completed over a period of time at Klepler Farm.

While measurements obtained in the HDO (shallow) and VDO (deep) followed similar trends in magnitudes, measurements obtained at the same observation points were not as closely similar ($r = 0.51$) as experienced in previous

studies. Because of this and the large number of negative readings in the HDO, the EM38DD meter has been returned to Geonics Limited for calibration and testing.

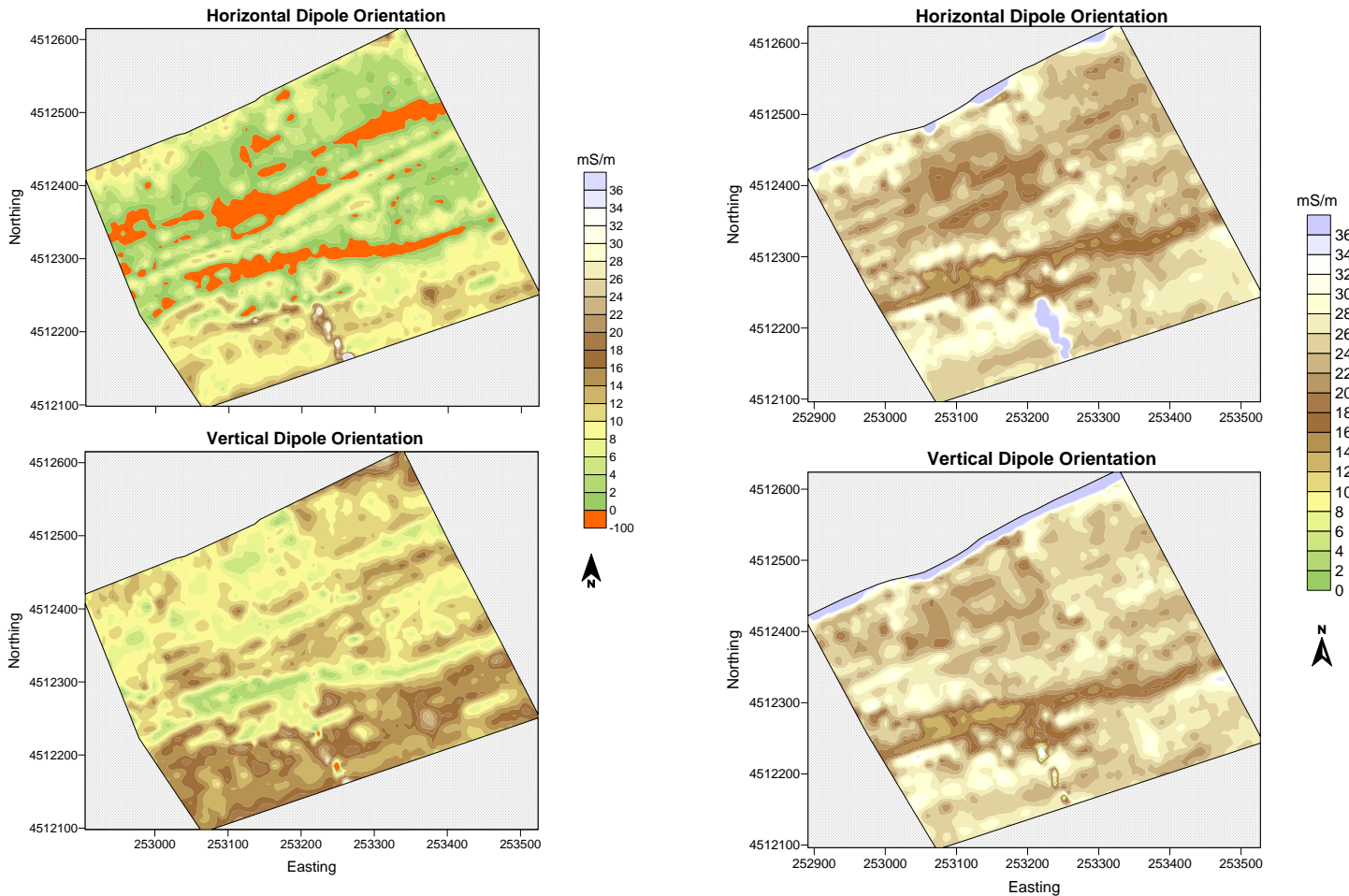


Figure 1. Plots of EC_a collected at Klepler Farm with the EM38DD meter operated in the horizontal (upper plots) and vertical (lower plots) dipole orientations. Surveys were conducted in March (left-hand plots) and January (right-hand plots) 2008.

Figure 1 contains four, two-dimensional plots of the EC_a data that were measured with the EM38DD meter in the horizontal (upper plots) and vertical (lower plots) dipole orientations for surveys completed in March (left-hand plots) and January (right-hand plots) 2008. In each plot, the isoline interval is 2 mS/m and the same color ramp is used. Spatial EC_a patterns appearing in Figure 1 appear to be principally related to differences in soil depth and wetness. Areas with lower EC_a are on higher-lying, more sloping, better drained landscape positions. In general, these areas have thinner caps of residuum and shallower depths to limestone bedrock. Areas with higher EC_a are on lower-lying, more imperfectly drained plane and concave slopes. In general, these areas are wetter, and have thicker caps of residuum and deeper depths to bedrock. In Figure 1, a prominent, east-to-west trending, linear band of lower EC_a can be identified in the lower center of each plot. This pattern closely conforms to the crest of a prominent ridgeline, where the depth to bedrock is mostly shallow. The extreme northeast portion of the study area was noticeably wetter at the time of both surveys. However, the inferred higher soil moisture contents in this portion of the study site did not translate into noticeably higher EC_a .

In the plots shown in Figure 1, the approximate locations of buried utility lines can be identified by anomalous EC_a values plotted along the northern boundary (mostly masked by blanking files) and in the extreme south central portion (most

evident in the upper plots) of the research fields. The northern portion of the field with the buried utility lines was avoided during the March survey.

Although similar spatial patterns are evident in each plot, a closer look reveals several troubling trends. EC_a was noticeably higher in January than in March (Table 1). Spatial patterns and absolute EC_a values for the January survey had been suspected of some error. As soils were considered wetter in March (or at least the surface layers), it was anticipated that EC_a would also be higher in March than in January. The lower EC_a in March can be attributed to the affects of partially frozen soil materials on EC_a or equipment errors (the EM38DD meter has been returned to Geonics Limited for calibration tests and maintenance). For the March survey, negative values were recorded in the HDO on some higher-lying, shallower to bedrock areas. While negative values are not in themselves disturbing [to me], greater care must be exercised in calibrating the EMI meter for the study of temporal variations in EC_a across these units of management. It is recommended that a know *meter calibration site* be established at Klepler Farm and more rigorous calibration standards be adopted. Some linear trends in EC_a patterns closely conform to the track of the ATV as it crossed the fields and to the locations of field boundaries. These trends represent artifacts (a wider isoline interval of 3 to 4 mS/m will reduce the impact of these artifacts). Data obtained in the VDO are considered more stable and a better reflection of spatial EC_a patterns than the data collected in the HDO.

2. Shale Hills Catchment:

Reconnaissance EMI Surveys:

Basic statistics for the four reconnaissance EMI surveys of the Shale Hills Catchment (October 2005, March 2006, January 2008, and March 2008) are listed in Table 2. All of these surveys were completed with the EM38 meter operated in the vertical dipole orientation. All EC_a measurements with negative values were removed from the data sets, as most were assumed to represent interference from metallic objects that are scattered throughout the catchment. At the time of the October 2005 survey, soils were noticeably droughty and stream flow was restricted to the stream channel in the lowest portion of the catchment. For the March 2006 survey, soils were considered moist and stream flow was observed in most reaches of the stream channel. Snow had recently melted from the catchment and the soils were moist at the time of the January 2008 survey. Recent rains and snow melts contributed to very moist conditions in the catchment at the time of the March 2008 survey. In general, with the exception of the March 2008 survey, results reflect these differences in soil moisture. In Table 2, the averaged EC_a can be seen to generally increase (with the exception of the March 2008 survey) with increasing soil moisture contents (OCT 2005 < MAR 2006 < JAN 2008 \geq March 2008).

Table 2
Comparison of Basic Statistics for the Reconnaissance EMI Surveys of the Shale Hills Catchment.

	October 2005	March 2006	January 2008	March 2008
Number Observations	5931	3448	6333	2810
Minimum	0.00	0.00	0.22	0.00
Maximum	23.75	20.50	26.00	29.56
25% Quartile	1.25	1.50	2.99	2.55
75% Quartile	3.00	5.78	6.84	5.32
Mean	2.22	3.94	5.06	4.23
Standard Deviation	1.38	3.20	3.06	2.76

Reception of satisfactory satellite signals was severely limited with the Trimble AG114 GPS receiver, and consequently the coordinates of many data points were not recorded. The non-reception of satellite signals was most noticeable along the lower reaches of the stream channel and along lower side slopes where vegetation and topography masked the signals. These areas typically have higher EC_a . In addition, satellite reception was poor along the eastern (west-facing slopes) side slopes of the catchment. The smaller data set collected during the March 2008 survey resulted in broader, less intricate EC_a patterns (see Figure 2, lower-right hand plot). In contrast to the previous three EMI reconnaissance surveys of the catchment, multiple traverses were not conducted across and along the swales. These landforms often had areas of higher EC_a . As a consequence of this sampling plan, the swales are indistinguishable on the plot of the March 2008 EC_a data.

Figure 2 contains plots of EC_a data collected in October 2005, March 2006, January 2008, and March 2008. In each of

these figures, the same color ramp and isoline interval (3 mS/m) have been used. These plots show the spatial distribution of EC_a data collected with the EM38 meter in the deeper-sensing (nominal penetration depth of 0 to 150 cm) vertical dipole orientation. In general, major spatial EC_a patterns appear temporally consistent. Typically, the lowest EC_a is recorded on plane and convex shoulder and back slopes. These soils (Wiekert and Berks) are characteristically drier and shallower to bedrock than other soils and landscape components within the catchment. Areas of higher EC_a are recorded along the stream channel. These soils (Earnest and Blair ton) are deeper and have higher moisture contents. In humid areas, EC_a is largely controlled by relatively stable soil properties (i.e., soil texture, density, and depth), but fluctuates in relative magnitude with changes in soil moisture contents. However, the effect of moisture variations on EC_a remains problematic within the Shale Hills Catchment. Lower than anticipated correlations have been observed between EC_a and volumetric moisture contents measured at time-domain reflectometry (TDR) monitoring sites. The complexity and short range variability of forested soil properties may be a contributing factor. Ken Takagi has already noted the need for more rigorous EMI protocol in this highly resistive environment.

As noted earlier, during the March 2008 survey, because of poor GPS reception, the amount of data recorded along lower side slopes and the stream channel was exceedingly sparse. Because of interpolations methods used during the construction of the computer simulation, these areas have been averaged based on the lower EC_a values recorded on higher-lying slope positions. As a consequence, the March 2008 survey does not show the higher EC_a that is so apparent along the stream channel of earlier surveys.

A large linear area of relatively high EC_a has developed on the convex shoulder slope of the south-facing side slopes at the time of the March 2008 survey. No explanation for this baffling pattern can be made at this time without further ground-truth observations or measurements. In relation to the previous surveys, the magnitude and location of this spatial pattern is highly anomalous.

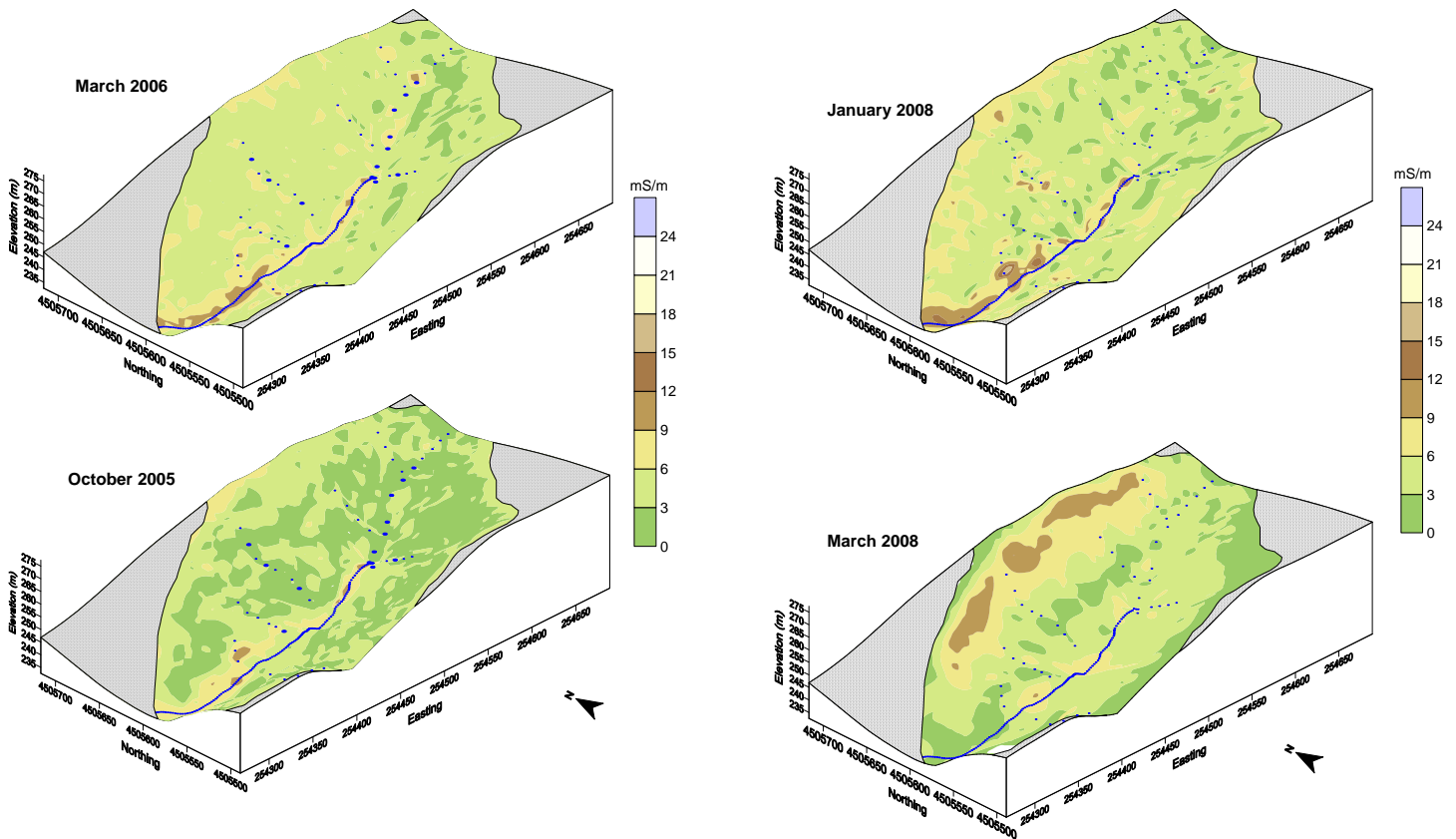


Figure 2. These plots show the spatial distribution of EC_a within the catchment at different times.

Ground-Penetrating Radar

In the absence of continuous and satisfactory outcrops or exposures, GPR is an excellent tool for imaging the regolith and bedrock (Cagnoli and Russell, 2000; and Dagallier et al., 2000). An emerging approach to GPR interpretations is three-dimensional (3D) visualization of GPR data (3D GPR). Three-dimensional GPR provides images that can improve our understanding of the structure and geometry of many subsurface features. Recently, with the advent of digital GPR outputs and advanced data processing software, it has become a routine practice to analyze the structure or configuration of subsurface features from a three-dimensional perspective. Grasmueck and Green (1996) noted that compared with the information provided by single 2D radar records, 3D GPR pseudo-images can provide “unrivaled resolution and detail of subsurface features”. Three-dimensional GPR pseudo-images allow the rapid viewing of the data volume from different cross-sections and directions (Beres et al., 1999).

Three dimensional GPR pseudo-images have been used to characterize sedimentary sequences and to better understand the internal structure and geometry of sedimentary rocks (Grasmueck et al., 2004; Szerbiak et al., 2004; Corbeanu et al., 2001a and 2002b; Junck and Jol, 2000; Asprien and Aigner, 2000 and 1997; Beres et al., 2000; and McMechan et al., 1997). Ground-penetrating radar is most effective in areas of coarse-textured unconsolidated materials. As a consequence, GPR has been frequently used to characterize the internal structure of dunes (Jol et al., 2002; Van Dam 2002; Bristow et al., 2000a and 2000b; Van Overmeeren, 1998; Gawthorpe et al., 1993; and Schenk et al., 1993). Methods of GPR facies analysis have been described for unconsolidated sediments (Beres and Haeni, 1991) and faults and fault zones (Green et al., 2003; Wyatt et al., 1996). Beres et al. (1999) discussed the potential of three-dimensional facies analysis using GPR and a limited number of exposures. These researchers used time-sliced images of 3D GPR pseudo-images to determine the strike of inclined layers and spatial relationships among different sedimentary structural units.

Unavoidably, the acquisition of data for 3D GPR pseudo-images requires greater expenditures of time and other resources than the collection of 2D radar records. To construct 3D GPR pseudo-images, a relatively small area (generally < 50 m²) is intensively surveyed with closely spaced (typically 0.1 to 0.5 m), parallel GPR traverse lines. The relatively dense network of traverse lines is necessary to resolve the geometries and sizes of different subsurface features and to prevent spatially *aliasing* of the data (Grasmueck and Green, 1996). The additional resources needed to collect and process GPR data for 3D imaging is often compensated for by more comprehensive spatial coverage and higher resolution of subsurface features (Grasmueck and Green, 1996).

In 3D GPR, data from closely-spaced, parallel lines are processed into a 3D GPR pseudo-image using software such as *GPR-Slice* or *RADAN*. Once processed, arbitrary cross-sections, insets, and time slices can be extracted from the 3D data set. Three-dimensional GPR imaging enables users to view the subsurface from nearly any perspective (Junck and Jol, 2000). Some software packages, allow the observer to rapidly travel through the entire data volume with animated imagery (Grasmueck, 1996). Interactive software packages permit the rapid display of any sub-section or block within the surveyed grid. The flexibility of 3D visualizations can greatly facilitate the interpretation of many spatial relationships and the analysis of lithologic and stratigraphic features. Lehmann and Green (1999) discuss considerations that are important for 3D GPR surveys. As noted by Szerbiak et al. (2001), all 3D GPR pseudo-images require correct velocity analysis (for reliable travel times to interfaces) and depth migration.

With two- and three-dimensional imaging of radar data, because of limited ground-truth observations, interpretations rest with the investigator's knowledge concerning the feature of interest. As noted by Regli et al. (2002) cores, outcrops, and geophysical information represents data of different quality and scale. Relationships between GPR patterns and subsurface structures are often ambiguous (Regli et al., 2002). Being more ambiguous than boring or outcrop data, 2D radar records and 3D GPR pseudo-images are considered soft data (Regli et al., 2002), which is interpretive and must be used with a caution.

Equipment:

The radar unit is the TerraSIRch Subsurface Interface Radar (SIR) System-3000, manufactured by Geophysical Survey Systems, Inc. (GSSI; Salem, NH).¹ The SIR-3000 consists of a digital control unit (DC-3000) with keypad, SVGA video screen, and connector panel. A 10.8-volt lithium-ion rechargeable battery powers the system. The SIR-3000 weighs about 9 lbs (4.1 kg) and is backpack portable. With an antenna, the SIR-3000 requires two people to operate. Daniels (2004) discusses the use and operation of GPR. A 400 MHz antenna was used in this investigation.

Radar records contained in this report were processed with the *RADAN* for Windows (version 6.6) software developed by GSSI.³ Processing included: header editing, setting the initial pulse to time zero, distance normalization, surface normalization, signal stacking, migration, and range gain adjustments. The Super 3D QuickDraw program developed by GSSI was used to construct three-dimensional (3D) pseudo-images of radar records collected at the grid site.

Field Methods:

To collect the data required for construction of 3D GPR pseudo-images, a survey grid was established on the lower portion of a swale within the Shale Hills Catchment. Two GPR surveys were conducted across this grid site: one survey with traverse lines parallel to the X-axis (cross swale profiles) and one survey with traverse lines parallel to the Y-axis (parallel the swale's long-axis). The grid site had overall dimensions of 4.0 by 5.0 m. Survey flags were inserted in the ground at 25 cm intervals along the four lines that defined the grid's outline. For the survey conducted parallel to the X-axis, the dimensions were only 4.0 m square. For the survey conducted parallel to the Y-axis, the survey covered the full of 4.0 by 5.0 m area. For each survey, successive GPR traverse lines were spaced 25 cm apart. A reference line (a distance-graduated rope) was stretched along the ground surface between matching survey flags on opposing sides of the grid. Distance marks were affixed to this reference lines at intervals of 100-cm. A 400 MHz antenna was towed along the graduated rope and, as it passed each 100-cm graduation, a mark was impressed on the radar record. Following data collection along a traverse line, the reference line was sequentially displaced 25-cm across the grid (to the next set of flags) to repeat the process. A total of 17 traverses were required to complete each GPR grid survey. Based on the depth to a known reflector (buried at a depth of 52 cm), the velocity of propagation (v) and relative dielectric permittivity (E_r) through the upper part of the soil profile were estimated. An E_r of 8.431 (v of 0.1026 m/ns) was used to depth scale the radar imagery.

Results:

The focus of signal processing is to reduce unwanted system noise and clutter, and to increase the interpretability of subsurface features appearing on radar records and images. The construction of 3D GPR pseudo-images requires multiple radar records. Typically, 2D radar records, which are collected parallel with the depositional or structural dip, show the greatest variation in form and are often the most impressive and informative (van Heteren et al., 1998). Some suggest that these traverses should be obtained both parallel and orthogonal to the dip of lithologic or stratigraphic features. Others suggest that the form and geometry of subsurface features can be studied in greater detail from two-dimensional, intersecting radar profiles (van Heteren et al., 1998). Figures 3 and 4 are 3D GPR pseudo-images of the grid site. Figure 3 is a 3D GPR pseudo-image prepared from data collected parallel to the X-axis. Figure 4 is a 3D GPR pseudo-image prepared from data collected parallel to the Y-axis (note the grid offset in the Y direction). In both images, an arbitrary 300 by 300 by 300 cm inset cube has been removed.

Radar records used to prepare the images shown in Figures 3 and 4 have been *terrain-corrected* or *surface normalized* to adjust for differences in elevation. Terrain correction is often used to improve visual presentations and interpretations. Through a process known as *surface normalization*, measured elevations are assigned to each reference point and the radar record is corrected for changes in relief. Surface normalization helps to improve the interpretative quality of 2D radar records and the association of subsurface reflectors with landscape components. However, in these 3D GPR pseudo-images constructed using *RADAN* software, the use of *surface normalization* results in some masking of the surface reflections, which are hidden behind the upper outline of the grid cube. It is anticipated that greater success will be had using *terrain corrected* radar records with *GPR-Slice*. In addition, in each 3D GPR pseudo-image (Figures 3 and 4), processing has resulted in one bordering Y or X traverse line to be misaligned with the remainder of the data set. The reasons for this misalignment are unclear at this time.

Radar records used to construct these 3D GPR pseudo-images were submitted to signal stacking and migration processing functions. Signal stacking (a signal averaging technique) is used to reduce high frequency noise. Migration is used to reduce diffraction tails of hyperbolic reflectors and to more properly position or align sloping interface. In addition, display gain adjustments were used to enhance subsurface reflections.

³ Manufacturer's names are provided for specific information; use does not constitute endorsement.

In the accompanying 3D pseudo-images, a sequence of stratigraphic layers is evident within the column of colluvium that fills the swale. These 3D pseudo-images do provide a means of visualizing and interpreting the 3D continuity of these layers. As radar scans are continuously collected in the direction of the radar traverse, subsurface features are better resolved along the direction of radar travel. In the direction orthogonal to the radar traverse, images are interpolated between successive GPR traverses. These images are therefore more poorly resolved and appear smudged. No significant differences in the interpretability of the two 3D pseudo-images are evident to me.

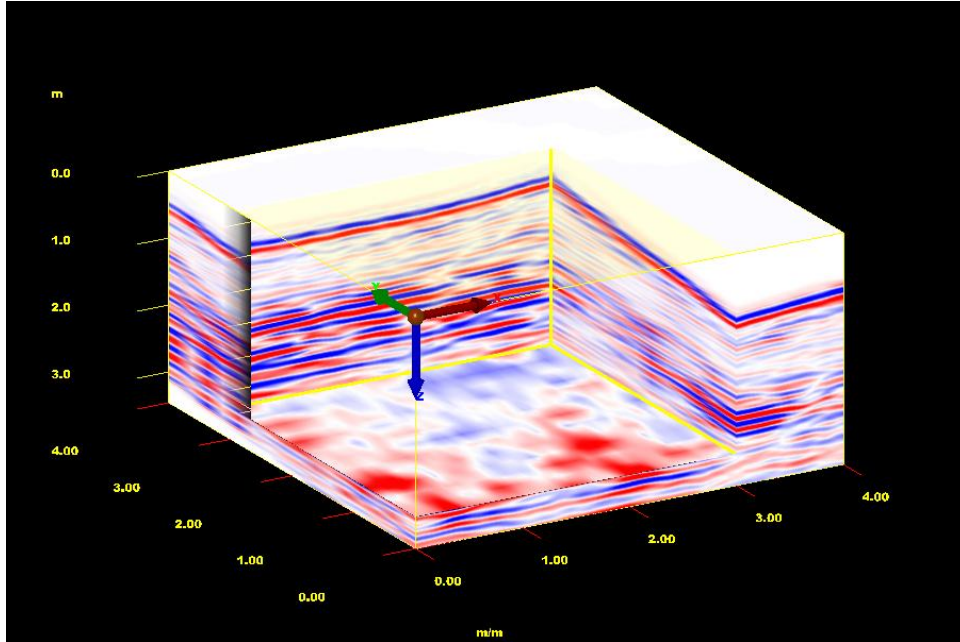


Figure 3. Three-dimensional pseudo image of the grid site. This grid was created from GPR traverses run parallel to X axis. In this image a 300 x 300 x 300 cm inset cube has been removed

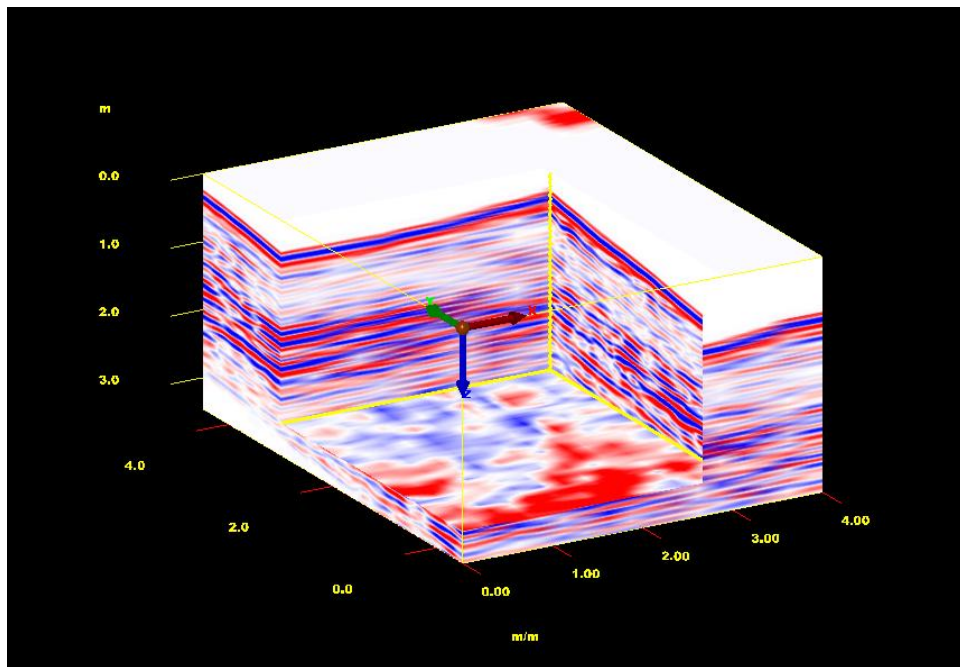


Figure 4. Three-dimensional pseudo image of the grid site. This grid was created from GPR traverses run parallel to Y axis. In this image a 300 x 300 x 300 cm inset cube has been removed.

Wetting Experiment:

An experiment was conducted to observe differences in subsurface reflection patterns associated with the infiltration of water in an area of Weikert soils. A metallic plate was buried at a depth of 22 cm and rested on the underlying shale bedrock surface. A three-meter traverse line was established across an area containing the buried plate. The estimated dielectric permittivity and velocity of propagation were 7.10 and 0.118 m/ns. Radar traverses were completed (1) before wetting, (2) immediately after wetting, (3) 15 minutes after wetting, and (4) 30 minutes after wetting. Wetting was accomplished by pouring 12.1 liters of water over the area immediately upslope from the buried metallic plate. During wetting water flowed across the soil surface to the refilled hole over the buried plate, but did not extend beyond this feature. The results of this study are shown in Figure 5. In general, wetting appears to dampen most subsurface reflection (even those downslope (to the right in Figure 5) of the refilled hole). Immediately after wetting, the diffraction tails from the buried metal disc achieve their high signal amplitudes. The diffraction tails appear to reduce in amplitude with time after wetting.

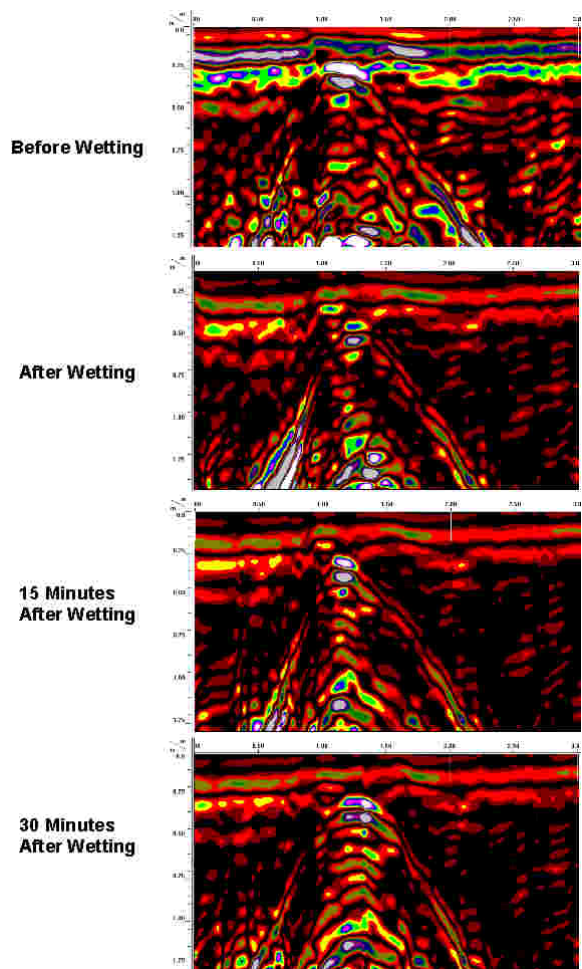


Figure 5. These 2D radar records show the results of a wetting experiment.

References:

Asprion, U., and T. Aigner, 1997. Aquifer architecture analysis using ground-penetrating radar: Triassic and Quaternary examples (S. Germany). *Environmental Geology*, 31(1/2): 66-75.

Asprion, U., and T. Aigner, 2000. An initial attempt to map carbonate buildups using ground-penetrating radar: an example from Upper Jurassic SW-Germany. *Facies*, 42: 245-252.

- Beres, M., A. G. Green, and A. Pugin, 2000. Diapiric origin of the Chessel-Noville Hills of the Rhone Valley interpreted from georadar mapping. *Environmental and Engineering Geoscience*, 6(2): 141-153.
- Beres, M., and F. P. Haeni, 1991. Application of ground-penetrating radar methods in hydrogeologic studies. *Ground Water*, 29: 375-386.
- Beres, M., P. Huggenberger, A. G. Green, and H. Horstmeyer, 1999. Using two- and three-dimensional georadar methods to characterize glaciofluvial architecture. *Sedimentary Geology*, 129: 1-24.
- Bristow, C. S., S. D. Bailey, and N. Lancaster, 2000a. The sedimentary structure of linear sand dunes. *Nature* 406:56-59.
- Bristow, C. S., P. N. Chroston, and S. D. Bailey, 2000b. The structure and development of foredunes on a locally prograding coast: insights from ground-penetrating radar surveys, Norfolk, UK. *Sedimentology* 47: 923-944.
- Cagnoli, B., and J. K. Russell, 2000. Imaging the subsurface stratigraphy in the Ubehebe hydrovolcanic field (Death Valley, California) using ground-penetrating radar. *Journal of Volcanology and Geothermal Research*, 96: 45-56.
- Corbeanu, R. M., G. A. McMechan, R. B. Szerbiak, and K. Soegaard, 2001a. Prediction of 3-D fluid permeability and mudstone distributions from ground-penetrating radar (GPR) attributes: Example from the Cretaceous Ferron member, east-central Utah. *Geophysics* 67(5): 1495-1504.
- Corbeanu, R. M., K. Soegaard, R. B. Szerbiak, J. B. Thurmond, G. A. McMechan, D. Wang, S. Snelgrove, C. B. Forster, and A. Menitove, 2001b. Detailed internal architecture of fluvial channel sandstone determined from outcrop, cores and 3-D ground-penetrating radar: Example from the middle Cretaceous Ferron sandstone, east-central Utah. *American Association of Petroleum Geologists Bulletin* 85(9): 1583-1608.
- Dagallier, G., A. I. Laitinen, F. Malartre, I. P. Van Campenhout, and P. C. H. Veecken, 2000. Ground penetrating radar application in a shallow marine Oxfordian limestone sequence located on the eastern flank of the Paris Basin, NE France. *Sedimentary Geology*, 130: 149-165.
- Daniels, D. J., 2004. *Ground Penetrating Radar*; 2nd Edition. The Institute of Electrical Engineers, London, United Kingdom.
- Gawthorpe, R. L., R. E. L. Collier, J. Alexander, M. R. Leeder, and J. S. Bridge, 1993. Ground penetrating radar: application to sand body geometry and heterogeneity studies. IN: North, C. P. and D. J. Prosser (eds.) *Characterization of fluvial and aeolian reservoirs*. Geological Society (London): 421-432.
- Geonics Limited, 1998. EM38 ground conductivity meter operating manual. Geonics Ltd., Mississauga, Ontario.
- Geonics Limited, 2000. EM38DD ground conductivity meter: Dual dipole version operating manual. Geonics Ltd., Mississauga, Ontario.
- Grasmueck, M., 1996. 3-D ground-penetrating radar applied to fracture imaging in gneiss. *Geophysics* 61(4): 1050-1064.
- Grasmueck, M. and A. G. Green, 1996. 3-D georadar mapping: Looking into the subsurface. *Environmental and Engineering Geoscience*, Vol II (2): 195-220.
- Grasmueck, M., R. Weger, H. Horstmeyer, 2004. Three-dimensional ground-penetrating radar imaging of sedimentary structures, fractures, and archaeological features at submeter resolution. *Geology* (32): 933-936.
- Green, A., R. Gross, K. Holliger, H. Horstmeyer, and J. Baldwin, 2003. Results of 3-D georadar surveying and trenching the San Andreas fault near its northern landward limit. *Tectonophysics* 368: 7-23.

- Hendrickx, J. M. H., V. Bouchers, D. L. Corwin, S. M. Lesch, A. C. Hilgendorf, and J. Schlue, 2002. Inversion of soil conductivity profiles from electromagnetic induction measurements. *Soil Sci. Soc. Am. J.* 66: 673-685.
- Jol, H. M., D. C. Lawton, D. G. Smith, 2002. Ground penetrating radar: 2-D and 3-D subsurface imaging of a coastal barrier spit, Long Beach, WA, USA. *Geomorphology* 1318:1-17.
- Junck, M. B. and H. M. Jol, 2000. Three-dimensional investigation of geomorphic environments using ground penetrating radar. 314-318 pp. IN: (Noon, D. ed.) *Proceedings Eight International Conference on Ground-Penetrating Radar*. May 23 to 26, 2000, Goldcoast, Queensland, Australia. The University of Queensland.
- Lehmann, F., and A. G. Green, 1999. Semiautomatic georadar data acquisition in three dimensions. *Geophysics*, 64(3): 719-731.
- McMechan, G. A., G. C. Gaynor, and R. B. Szerbiak, 1997. Use of ground-penetrating radar for 3-D sedimentological characterization of clastic reservoir analogs. *Geophysics*, 62(3): 786-796.
- Regli, C., P. Huggenberger, and M. Rauber, 2002. Interpretation of drill core and georadar data of coarse gravel deposits. *Journal of Hydrology*, 255: 234-252.
- Szerbiak, R. B., G. A. McMechan, R. Corbeanu, C. Forster, and S. H. Snelgrove, 2001. 3-D characterization of a clastic reservoir analog: from 3-D GPR data to a 3-D fluid permeability model. *Geophysics*, 66(4): 1026-1037.
- Schenk, C. J., D. L. Gautier, G. R. Olhoeft, and J. E. Lucius, 1993. Internal structure of an aeolian dune using ground-penetrating radar. *International Association of Sedimentologists. Special Publication 16*: 61-69.
- U.S. Salinity Laboratory Staff, 1954. *Diagnosis and improvement of saline and alkali soils*, USDA Handbook 60. U.S. Government Printing Office, Washington, DC, USA.
- Van Dam, R. L., 2002. Internal structure and development of an aeolian river dune in The Netherlands, using 3-D interpretation of ground-penetrating radar data. *Netherlands Journal of Geosciences* 81 (1): 27-37.
- van Heteren, S., D. M. Fitzgerald, P. A. McKinlay, and I. V. Buynevich, 1998. Radar facies of paraglacial barrier systems: coastal New England, USA. *Sedimentology*, 43: 181-200.
- Van Overmeeren, R. A., 1998. Radar facies of unconsolidated sediments in The Netherlands: A radar stratigraphy interpretation method for hydrogeology. *Journal of Applied Geophysics* 40: 1-18.
- Wyatt, D. E., M. G. Waddell, and G. B. Sexton, 1996. Geophysics and shallow faults in unconsolidated sediments. *Ground Water*, 34: 326-334.